International Journal of Heat and Fluid Flow 000 (2016) 1–9

Contents lists available at ScienceDirect

International Journal of Heat and Fluid Flow

journal homepage: www.elsevier.com/locate/ijheatfluidflow

Effect of Prandtl number on the linear stability of compressible Couette flow

Ashwin Ramachandran [a], Bijaylakshmi Saikia [a], Krishnendu Sinha [a,*], Rama Govindarajan [b]

[a] Indian Institute of Technology Bombay, Mumbai, 400076, India
[b] TIFR Centre for Interdisciplinary Sciences, Hyderabad, 500075, India

ARTICLE INFO

Article history:
Received 17 October 2015
Revised 17 June 2016
Accepted 30 June 2016
Available online xxx

Keywords:
Compressibility
Mach number
Transport property
Acoustic modes
Mode-synchronization

ABSTRACT

Accurate prediction of laminar to turbulent transition in high-speed flows is a challenging task. Compressibility, and the resultant large variations in the transport properties can affect the transition process significantly. In this paper, we study the influence of Prandtl number, the ratio of momentum to heat diffusivity, in Couette flows at high Mach numbers. It is a part of an ongoing research programme to isolate and understand the transport property effects on the stability of high-speed flows. As a first step, we neglect the high-temperature effects and vary the Prandtl number in the range 0.9 to 0.2, by changing the relative magnitudes of viscosity and conductivity. A temporal linear stability analysis shows that the variation of phase speed with Prandtl number leads to synchronization between two acoustic modes, with peaks in growth rate at the synchronization points. Two types of branching patterns are observed depending on the Prandtl number, and the branch type determines which of the two modes is destabilized and which one is stabilized due to synchronization. Further, the mode shapes are either retained as earlier or interchanged between the two acoustic modes depending on the branching pattern. The stability diagrams for varying Mach and Reynolds numbers show a destabilizing role of decreasing the Prandtl number, both in terms of increased disturbance growth rates, and of larger regions of instability in the parameter space. It also results in a significant reduction in the critical Reynolds number of the flow, especially at high Mach numbers with wall cooling.

1. Introduction

To predict the transition from laminar to turbulent flow has been one of the most challenging problems concerning the applied fluid mechanics community for many decades. At high speeds, compressibility brings in additional physics which affects the laminar-turbulent transition (Reshotko, 1960; Mack, 1987; Xie and Girimaji, 2014). Transport properties, like viscosity and thermal diffusivity, vary with temperature and pressure, especially close to the wall, for a compressible flow. The Prandtl number, which is the ratio of kinematic viscosity to thermal diffusivity can vary significantly, especially at high temperature conditions. The variation of transport properties, including the Prandtl number, and their effect on the stability of high-speed flows have been reported previously (Lyttle and Reed, 2005; Franko et al., 2010).

Extensive work has been carried out to investigate the physical effects of transport properties on the stability of incompressible as well as compressible flows. For example, Wall and Wilson (1997) examine the effect of different viscosity models on the stability of incompressible boundary layers. They find that a non-uniform decrease in viscosity across the boundary layer stabilizes the flow, and the extent of stabilization increases as the Prandtl number is increased. In another work, Sameen and Govindarajan (2007) report a destabilizing effect of Prandtl number on the transient growth of instabilities for incompressible channel flows.

In the context of compressible flows, Hu and Zhong (1998) examine the effect of viscosity on the linear stability of plane Couette flow by comparing with the inviscid results of Duck et al. (1994). They find that viscosity plays a destabilizing role on the first two acoustic modes for a range of Reynolds numbers and wave numbers. Malik et al. (2008) study the effect of viscosity stratification, by comparing with a Couette flow with uniform values of transport properties. They report that the stratification of viscosity can significantly stabilize the flow. A constant Prandtl number is assumed in their work, which implies that viscosity and thermal conductivity are proportional and they vary together. This may not be the case in many high-speed flows, where the transport and the thermodynamic properties have large independent variations with

* Corresponding author.
E-mail address: krish@aero.iitb.ac.in (K. Sinha).

http://dx.doi.org/10.1016/j.ijheatfluidflow.2016.06.014

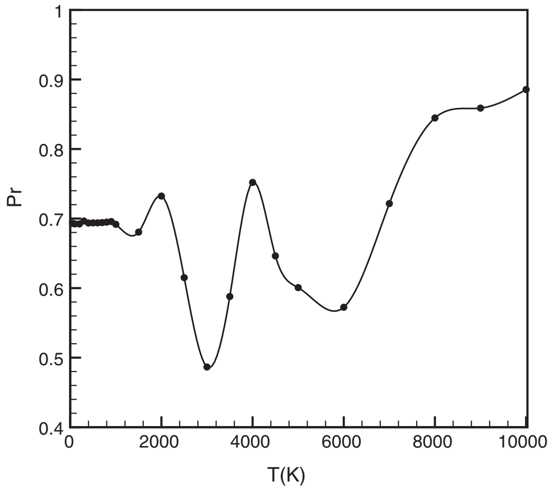

Fig. 1. Variation of Prandtl number for equilibrium air with temperature at 1 bar pressure (Data taken from Capitelli et al. (2000)).

temperature and pressure, resulting in large non-monotonic variation of Prandtl number. Fig. 1 shows the variation of Prandtl number for air at local thermodynamic equilibrium, over a range of temperatures. The data is taken from Capitelli et al. (2000) and calculated using perturbative Chapman-Enskog method. The minimum value of Prandtl number (0.49) is observed at a temperature around 3000 K, while the highest value (0.89) is observed at 10, 000 K. The data corresponds to 1 bar pressure, and the Prandtl number may attain even lower values at lower pressures typical of high-altitude conditions. Therefore, we consider Prandtl numbers from 0.2 – 0.9 for the cases studied in this paper.

The objective of our work is to isolate and understand the effects of mean viscosity and thermal conductivity, their relative magnitude and stratification on the stability of compressible flows. The current paper is a step in this direction and it focuses on the effect of Prandtl number on the nature and growth of disturbances at varying Mach and Reynolds numbers. In a related work (Saikia et al., 2016), we study the effect of the variation of Prandtl number across a shear layer, due to changes in the transport properties with temperature. The variation of viscosity and conductivity is seen as a combination of a change in their magnitude, superimposed by a gradient across the flow. It is found that viscosity stratification strongly stabilizes the flow, whereas conductivity stratification has a mixed effect depending on the Mach number of the flow. Additionally, the changes in the relative magnitudes of viscosity and conductivity is found to play a vital role and this motivates the current paper.

We ask, how much does the ratio of diffusivities affect the stability, all other factors held the same? To answer this question, we consider the two-dimensional compressible plane Couette flow as our model problem. This flow configuration has been studied extensively and it helped bring out significant fundamental physics related to flow instability and transition. Plane Couette flow affords a constant shear and is thus the simplest shear flow we may consider. This geometry has been used in the previous works to study the effect of transport properties (Hu and Zhong, 1998; Malik et al., 2008), and our findings can thus be compared directly to the existing results. In a related work (Ramachandran et al., 2015), we have investigated the effect of Prandtl number on the stability of high-speed boundary layer flows.

We assume uniform viscosity and thermal conductivity throughout the flow field and vary the Prandtl number of the gas systematically. The variation of the Prandtl number is carried out by changing the relative magnitudes of viscosity and conductivity. Although the values of these transport properties are constant across a flow, they vary between two Couette flows with different Prandtl numbers. The thermodynamic properties, including specific heat of the gas, are kept constant and this is consistent with the perfect gas assumption used in this work. A constant property flow, such as the one we study here, is a theoretical construct, which enables us to eliminate the effects of transport property stratification that can have additional influence on stability (Malik et al., 2008; Saikia et al., 2016). We can thus isolate the physical effects of Prandtl number on the stability characteristics of compressible plane Couette flow, which is the objective of this paper. In compressible flows, the Prandtl number is usually less than 1, which means that heat diffuses faster than momentum. We show that the ratio of their diffusivities can have a large effect on the stability margins of a compressible flow.

The variations in Prandtl number in high-speed flows are often associated with high-temperature phenomena, like chemical reactions and internal energy excitation. The effects of non-equilibrium thermo-chemistry on flow stability has been studied extensively (Malik and Anderson (1991); Hudson et al. (1997); Johnson et al. (1998) and others). For example, Malik and Anderson (1991) show that real-gas effects stabilize the first mode and destabilize the second mode instabilities in boundary layer flows. In another work, Franko et al. (2010) report significant differences in the frequency and growth rates due to variations in thermo-chemical and transport properties, including Prandtl number. In the current work, we find a strong destabilizing effect of the Prandtl number in high Mach number perfect gas flows. As a first step, we have neglected the high-temperature phenomena so as to isolate the effect of Prandtl number on flow stability. A complete study of transport property effects, including the Prandtl number variation, will require additional modeling of non-equilibrium thermo-chemistry at high-temperature conditions.

We clarify that real-life compressible flows have myriad competing effects, and there is no way in an experiment to isolate the effects of Prandtl number alone. We also caution the reader that the present results are for the simplest of shear flows, namely a Couette flow, and are not trivially extendable to other geometries. However, given that the effective Prandtl number in a realistic high-Mach-number flow depends on temperature and composition in a non-trivial way, our contribution that lower Prandtl numbers are indicative of higher levels of instability could be of value to those studying more complex situations. We hope that these findings will motivate those working on realistic compressible flows to examine whether heat diffusing faster than momentum can indeed be a source of destabilization.

We apply linear stability theory to compressible Couette flow with different Prandtl numbers. Formulation of the base flow and details of the temporal stability analysis are described in Sections 2 and 3 respectively. Section 4 presents the effect of Prandtl number on mode synchronization. Stability diagrams for varying Mach numbers and Reynolds numbers are presented in Sections 5 and 6 respectively. Additional results pertaining to wall cooling/heating at different Prandtl numbers are also reported (Section 7), and are followed by conclusions.

2. Base flow

A perfect Newtonian gas is confined between two infinite parallel plates separated by a distance L_∞. The bottom wall is stationary and the top wall moves with a velocity U_∞. The streamwise, wall-normal and spanwise velocities are represented by u, v and w respectively. The subscript ∞ is used to denote the upper-wall quantities, whereas mean flow variables are represented by overbar.

The three-dimensional unsteady compressible Navier-Stokes equations are used to describe the flow, where the length and time scales are non-dimensionalized by L_∞ and L_∞/U_∞ respectively. All other flow variables are non-dimensionalized by their corresponding top-wall values. The dimensionless parameters are:

$$Re = \frac{\rho_\infty U_\infty L_\infty}{\mu_\infty}, \quad Pr = \frac{\mu_\infty C_p}{\kappa_\infty}, \quad M = \frac{U_\infty}{\sqrt{\gamma R T_\infty}}. \tag{1}$$

Here, *Re, Pr* and *M* represent the Reynolds number, Prandtl number and Mach number respectively. Temperature, specific gas constant, density, specific heat at constant pressure and the ratio of specific heats are represented by *T, R,* ρ, C_p and γ respectively. Viscosity and conductivity are denoted by μ and κ, and $\gamma = 1.4$ is assumed.

The generalized non-dimensional form for the three-dimensional unsteady Navier-Stokes equations can be found in Malik (1990). For obtaining the governing equations for a plane Couette flow with uniform viscosity ($\bar{\mu} = 1$) and thermal conductivity ($\bar{\kappa} = 1$), the base flow is assumed to be steady and unidirectional. This leads to identically zero solutions for the continuity and *z*-momentum equations, and the *y*-momentum equation provides a constant pressure condition ($\bar{p} = 1$). The *x*-momentum and energy equations simplify to:

$$\frac{d\bar{u}}{dy} = \text{constant}, \tag{2}$$

$$\frac{d}{dy}\left(\frac{d\bar{T}}{dy}\right) + (\gamma - 1)M^2 Pr \left(\frac{d\bar{u}}{dy}\right)^2 = 0. \tag{3}$$

Boundary conditions: Velocity satisfies the no-slip condition at both walls. The temperature boundary conditions imposed on the upper and lower walls are isothermal and adiabatic respectively, i.e.

$$\bar{u}(0) = 0; \quad \bar{u}(1) = 1, \tag{4}$$

$$\frac{d\bar{T}}{dy}(0) = 0; \quad \bar{T}(1) = 1. \tag{5}$$

By making use of the velocity boundary conditions, Eq. 2 reduces to $\bar{u} = y$. Substituting the velocity profile into Eq. 3, we integrate it and use the temperature boundary conditions to obtain the following expression for temperature as a function of *y*.

$$\bar{T} = 1 + \frac{(\gamma - 1)M^2 Pr}{2}\left(1 - y^2\right). \tag{6}$$

3. Linear stability equations

Linear stability equations for the perturbations are derived by representing the instantaneous flow variable (A) as a sum of the mean flow variable ($\bar{A}$) and a small fluctuation quantity ($\tilde{A}$), i.e.,

$$A = \bar{A}(y) + \tilde{A}(x, y, z, t). \tag{7}$$

Substituting Eq. 7 into the non-dimensional form of the governing equations and neglecting the higher-order and non-linear terms, we obtain the linearized perturbation equations. The fluctuations are expressed in a normal mode form,

$$\tilde{A}(x, y, z, t) = \hat{A}(y) e^{i(\alpha x + \beta z - \omega t)}, \tag{8}$$

where, $\hat{A}(y)$ represents the complex amplitude of the flow variable of a traveling wave with wave number components α, β in the $x - z$ plane and frequency ω. We consider a temporal stability problem with $\omega = kc$, where $k = \sqrt{\alpha^2 + \beta^2}$, and c represents the phase speed of the disturbance wave. The frequency ω is assumed to be complex and both α and β are real. We substitute the perturbed form (Eq. 8) into the linearized disturbance equations to obtain a homogeneous system of ordinary differential equation, which can be expressed as,

$$B\psi = \omega I \psi. \tag{9}$$

Here, $\psi = (\hat{u}, \hat{v}, \hat{w}, \hat{\rho}, \hat{T})^{tr}$ is the vector of the complex amplitudes of the flow variables and I is the identity matrix. B is a $5N \times 5N$ (N is the number of Chebyshev points) complex matrix, and its elements are functions of α, β, *Re, Pr, M* and the mean-flow variables. The entries of matrix B are listed in the appendix.

Boundary conditions on the perturbations are applied at both walls. The velocity fluctuations satisfy the no-slip condition at the walls, i.e.

$$\hat{u}(0) = \hat{u}(1) = \hat{v}(0) = \hat{v}(1) = \hat{w}(0) = \hat{w}(1) = 0. \tag{10}$$

At the upper wall, isothermal boundary condition is imposed for the temperature fluctuations and at the lower wall adiabatic condition is satisfied.

$$\hat{T}(1) = 0, \quad \frac{d\hat{T}}{dy}(0) = 0. \tag{11}$$

To obtain the boundary condition for the density perturbation, the *y*-momentum equation is solved at the walls. With the help of these boundary conditions, a Chebyshev spectral collocation method (Trefethen, 2000) is used and the resulting eigenvalue problem (Eq. 9) is solved numerically using the QZ algorithm of MATLAB. This provides the complex frequency $\omega = \omega_r + i\omega_i$, where ω_i represents the growth or decay rate of the disturbance wave.

We have validated our code by computing a case from Hu and Zhong (1998) with parameters $M = 2$, $Re = 2 \times 10^5$ and $\alpha = 0.1$. The results computed using 100 Chebyshev points match up to four decimal places with the data mentioned in Hu and Zhong (1998). Further, the results presented in this paper are grid converged and computed using $100 - 150$ points.

Note that the majority of the results in this work are obtained using the temporal stability analysis described above. The only exception is the mode synchronization described in section 4.1 and 4.2. Here, we need a spatio-temporal analysis, where both the disturbance frequency and wave number are assumed to be complex. This is required because it is not possible to find all the branch points in the real wave number plane (see Federov and Tumin (2011)).

4. Eigenspectrum: Mode synchronization

The parameters which govern the stability characteristics of compressible Couette flow are Mach number, Reynolds number, Prandtl number and the wavenumber of the disturbance. The effect of *M, Re* and wave number on flow stability have already been studied in Hu and Zhong (1998). Here, we quantify the effect of Prandtl number on the eigenspectrum.

Fig. 2 plots the real (c_r) and imaginary (c_i) parts of the temporal eigenvalues for a Mach 12, $\alpha = 5$ and $Re = 10^5$ plane Couette flow with two-dimensional disturbances ($\beta = 0$). The set of eigenvalues which appear in the **Y** shaped branch in Fig. 2 correspond to

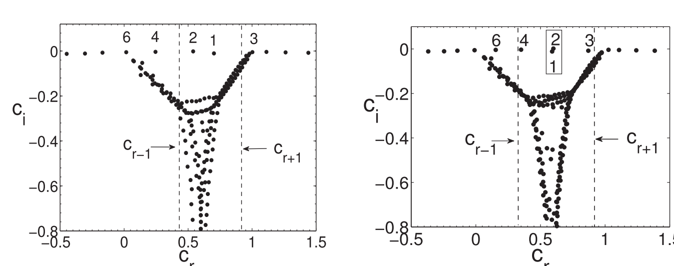

(a) $Pr = 0.9$ (b) $Pr = 0.5$

Fig. 2. As the Prandtl number is reduced, the odd and even acoustic modes approach each other leading to the synchronization of the first two acoustic modes 1 and 2 (marked by a rectangular box), for a $M = 12$, $Re = 10^5$, $\beta = 0$ and $\alpha = 5$ flow. The two dashed lines encompass the acoustic modes with two relative sonic lines.

the viscous modes. The discrete modes observed on top of the viscous modes with $c_i \simeq 0$ are the acoustic modes (Duck et al., 1994), and the first few are numbered for reference. As the Prandtl number is reduced from 0.9 to 0.5, the phase speed of the odd acoustic modes decrease, while it increases significantly for the even modes. A synchronization between the first two acoustic modes is observed when their phase speeds are comparable (identified by the rectangular box in Fig. 2(b)). It is found that such synchronizations can result in high growth rates, which often lead to dominant instabilities in the flow.

Synchronization between the acoustic modes has been presented in Federov and Tumin (2011) for high Mach number flat plate boundary-layer flows. They observe two types of discrete modes in the boundary layer – fast and slow modes, and when these modes synchronize, a branching of the discrete spectrum is observed. It is shown that the eigenvalues attain complex conjugate values around the synchronization point, and the eigenmodes display identical profiles across the boundary layer. We see similar trends in the eigenvalues and eigenfunctions in compressible Couette flow, and the branching patterns observed for different values of Prandtl numbers are described next.

4.1. Branching pattern at high Prandtl numbers

Fig. 3(a) plots the variation of phase speed and growth rate with wavenumber for the first four acoustic modes at $M = 12$, $Re = 10^5$ and $Pr = 0.5$. The wavenumber is varied from around 4.5–9.6 and the arrows in the figure indicate the direction of increasing wavenumber. When the wavenumber is around 4.8, we observe the first synchronization between the first two acoustic modes around a phase speed of 0.6. A magnified view of this synchronization is presented in Fig. 3(b). When the wavenumber is increased progressively, these two modes cross one another and they encounter the higher modes at comparatively larger wavenumbers. Synchronizations between modes 1 and 4, and 2 and 3 are also observed in the range of wavenumbers considered. We notice local peaks and dips in the growth rates during these synchronizations.

The branching pattern observed during synchronization between modes 1 and 2 is presented in Figs. 3(c) and 3(d). The phase speed plotted as a function of the disturbance wavenumber shows a monotonic decrease for mode 1. The phase speed of mode 2 increases continuously and they attain matching values at a wavenumber of 4.77. Synchronization between the modes makes mode 2 more unstable, and mode 1 gets highly stabilized. We term this branching pattern as “cross-over” branching, and is observed in compressible Couette flow at relatively high Prandtl numbers.

For the compressible boundary layer flows considered by Federov and Tumin (2011), the branch points are plotted in the complex wavenumber plane (see Fig. 15 in their work). We perform a similar spatio-temporal study for the present flow in the vicinity of mode synchronization. Since all the branch points can not be located using temporal stability analysis in the real wavenumber plane, we have to use spatio-temporal analysis in the complex wave number plane. Further details can be found in Federov and Tumin (2011). Though the Couette flow considered in this work is x-homogeneous, a disturbance can grow or decay as it is convected downstream. This corresponds to the imaginary part of the wavenumber being negative ($\alpha_i < 0$) or positive ($\alpha_i > 0$), respectively. When the branch points are located in the lower half plane ($\alpha_i < 0$), the solution marching along the real wavenumber axis bypasses the branch points from above. This is identified as branching pattern **B** in Federov and Tumin (2011) and is identical to the cross-over branching discussed above. The two branching points for this case are located at $\alpha_r = 4.77,\ \alpha_i = -0.005$ and $\alpha_r = 4.94,\ \alpha_i = -0.179$ respectively. The synchronization pattern between higher modes (1 and 4, and 2 and 3) also exhibit cross-over branching pattern, similar to the one between the first two acoustic modes.

4.1.1. Eigenfunctions

As reported in Hu and Zhong (1998), the peak in the pressure eigenfunction appears close to the top wall for even acoustic modes, and at the bottom wall for the odd modes. It is noted that high-amplitude perturbations appear in an embedded region of local supersonic flow relative to the phase speed of the instability wave. The relative Mach number, defined as $M_r = \frac{\bar{u}-c_r}{\sqrt{\bar{T}}}M$, is used to identify the relative supersonic regions for each mode in a given Couette flow.

In general, acoustic modes have only one relative sonic line (if any), with the odd modes having $M_r = -1$ and $M_r = 1$ for the even modes. But in certain cases, for example, modes 1 and 2 in Fig. 2(a), and the first four acoustic modes in Fig. 2(b), there are two relative sonic lines. The condition for the odd modes to have the second relative sonic line, i.e., $M_r = 1$ is that the phase speed of the disturbance should satisfy $c_r \le \bar{u} - \frac{\sqrt{\bar{T}}}{M}$, at the upper wall. Since the values of $\bar{u}$ and $\bar{T}$ are 1 at the upper wall, the phase speed of the limiting disturbance becomes $c_{r+1} = 1 - \frac{1}{M}$. This gives the upper bound on the phase speed of the odd modes to have two relative sonic lines and is marked by a vertical dashed line in Fig. 2. Similarly, for the even modes to have the second relative sonic line ($M_r = -1$), they must satisfy $c_r \ge \bar{u} + \frac{\sqrt{\bar{T}}}{M}$, at the lower wall, which yields, $c_{r-1} = \sqrt{\frac{1}{M^2} + \frac{(\gamma-1)Pr}{2}}$. This expression gives the lower bound on the phase speed of the even modes to have two relative sonic lines, and is marked by a second vertical dashed line in Fig. 2.

The disturbance phase speed c_{r+1} corresponding to $M_r = 1$ for the odd modes is only a function of the reference Mach number. Therefore when we decrease the Prandtl number from 0.9 to 0.5 (refer Fig. 2), c_{r+1} remains constant at a value of 0.9167. However,

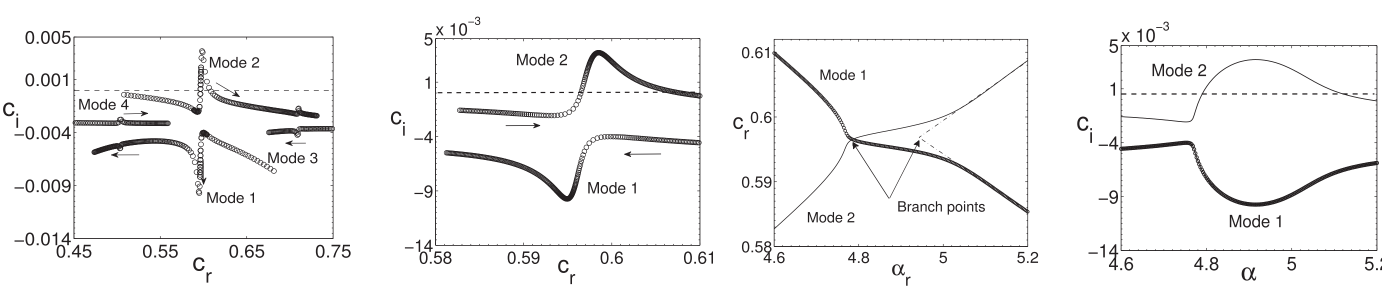

(a) Eigenvalues (b) Magnified view (c) Phase speed (d) Growth rate

Fig. 3. Variation of the phase speed and growth rate with wavenumber plotted for the first few acoustic modes at $M = 12$, $Re = 10^5$ and $Pr = 0.5$, showing synchronization of modes characterized by matching phase speeds and local peaks/dips in the growth rates. Arrows in (*a*) and (*b*) indicate the direction of increasing wavenumber, and the data in (*c*) is extrapolated back in α_r to locate the second branch point.

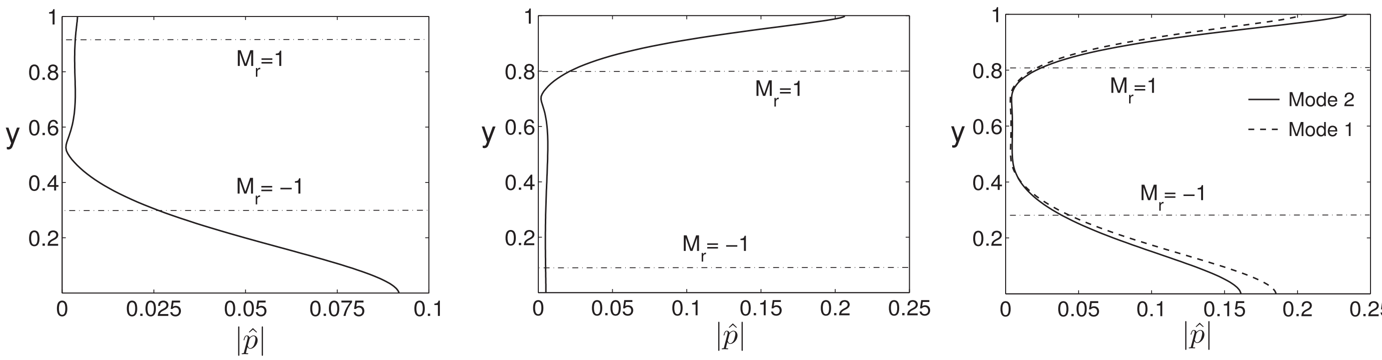

(a) Mode 1 (b) Mode 2 (c) Mode 1 and 2

Fig. 4. Pressure eigenfunctions plotted as a function of the wall normal coordinate show high amplitudes in the regions of relative supersonic flow. Data corresponds to (*a*) mode 1 and (*b*) mode 2 for the parameters used in Fig. 2(a), and (*c*) modes 1 and 2 for the parameters corresponding to the synchronization in Fig. 2(b).

the phase speed c_{r-1} corresponding to $M_r = -1$ for the even modes is a function of the reference Mach number and the Prandtl number. Its value decreases from 0.4324 to 0.327 as *Pr* is reduced. Thus, the range of wave speeds bounded by the two limiting values increase with decreasing Prandtl number and more acoustic modes are observed with two relative sonic lines at lower Prandtl numbers compared to a higher Prandtl number case (compare Fig. 2(a) and (b)).

The location of relative sonic lines along with the pressure eigenfunctions for the first two acoustic modes in Fig. 2(a) are shown in Fig. 4(a) and (b). We observe that for mode 1, the amplitude of the pressure eigenfunction increases in the relative supersonic region close to the bottom wall, bounded by the sonic line $M_r = -1$, and reaches a maximum value at the bottom wall (see Fig. 4(a)). On the other hand, for mode 2, an increase in the pressure eigenfunction is noticed in the relative supersonic region close to the top wall, bounded by the other sonic line $M_r = 1$, and the maximum amplitude is attained at the top wall (see Fig. 4(b)). The pressure eigenfunctions corresponding to the synchronization between the first two acoustic modes are shown in Fig. 4(c). We observe high amplitudes in the pressure eigenfunctions in the relative supersonic regions close to both the walls, bounded by the respective sonic lines. The variation of the eigenfunctions across the shear layer are almost identical for both the modes, when their phase speeds are close. Similar patterns for the eigenfunctions at the synchronization between the fast and slow modes in a high-speed flat plate boundary layer flow are reported in Federov and Tumin (2011) (see Figs. 23 and 24 in their paper).

4.2. Branching pattern at low Prandtl numbers

Fig. 5(a) presents the synchronization pattern obtained at $M = 12$, $Re = 10^5$ and a Prandtl number of 0.4. We plot the phase speed and growth rates of the first four acoustic modes and once again, track their variation with increasing wavenumber. High growth rates are observed at the synchronization points similar to that shown in Fig. 3(a). However, we notice a prominent difference in the branching pattern corresponding to the synchronization between the acoustic modes 1 and 2 as compared to the higher Prandtl number (= 0.5) case. A magnified view is presented in Fig. 5(b) as these two modes approach each other when the wavenumber is increased. The closest phase speed between the modes is attained at $\alpha_r = 4.19$, beyond which they revert back and move away. Modes 1 and 2 do not cross over as seen in Fig. 3(b).

We refer to the branching pattern at low Prandtl numbers as the “revert-back” branching, where the phase speeds of the two modes show non-monotonic behavior with increasing wave number. Mode 1, as expected, has a higher phase speed than mode 2, initially. After synchronization, the phase speed of mode 1 increases again with wave number to attain values higher than mode 2 (see Fig. 5(c)). This is opposite to the trend seen in the “cross-over” branching at higher Prandtl number (Fig. 3(c)). Also, the growth rate of mode 1 shows a sharp increase during synchronization and there is a corresponding decrease in the growth rate of mode 2 (see Fig. 5(d)). On the contrary, mode 2 is destabilized due to synchronization with mode 1 (see Fig. 3(d)) at higher Prandtl numbers.

The variation of phase speed plotted as a function of wavenumber (Fig. 5(c)) shows that the phase speed of the first two acoustic modes do not match for any real wavenumber value. However a synchronization point is noticed in the complex wavenumber plane corresponding to $\alpha_r = 4.19$ and $\alpha_i \simeq 0.0044$. A second synchronization point is obtained at $\alpha_r = 4.45$ and $\alpha_i \simeq -0.115$ by extrapolating back in α_r, as shown in Fig. 5(c). As we march along the real wavenumber axis, the first synchronization point ($\alpha_i > 0$) has to be bypassed from below, and the second synchronization point

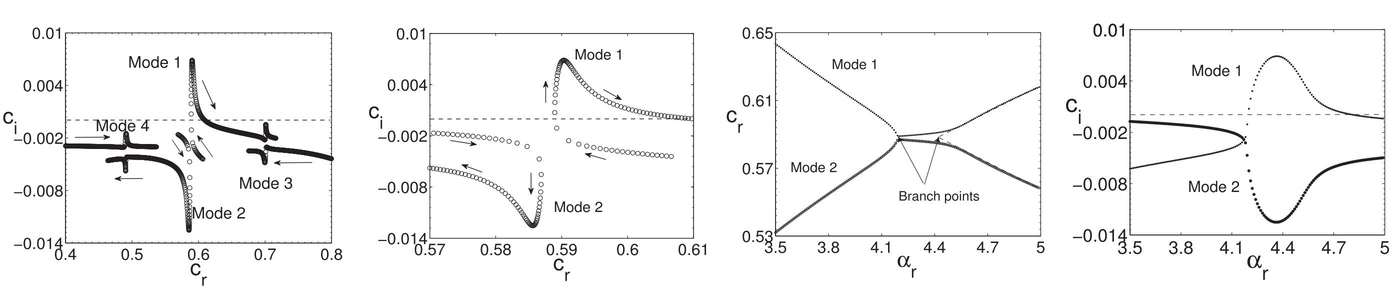

(a) Eigenvalues (b) Magnified view (c) Phase speed (d) Growth rate

Fig. 5. Variation of growth rate and phase speed with wavenumber for the first few acoustic modes at $M = 12$, $Re = 10^5$ and $Pr = 0.4$. Modes 1 and 2 do not attain a common phase speed, but the higher modes 3 and 4 synchronize with modes 1 and 2 respectively. Increase in wavenumber is shown by the direction of arrows.

Please cite this article as: A. Ramachandran et al., Effect of Prandtl number on the linear stability of compressible Couette flow, International Journal of Heat and Fluid Flow (2016), http://dx.doi.org/10.1016/j.ijheatfluidflow.2016.06.014

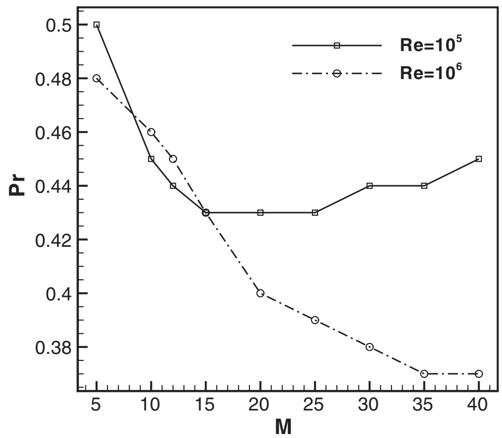

Fig. 6. The threshold Prandtl number dividing the two branching patterns i.e., "cross-over" (at high *Pr*) and "revert-back" (at low *Pr*) as a function of Mach number at two Reynolds numbers $Re = 10^5$ and $Re = 10^6$. Data corresponds to the synchronization between the acoustic modes 1 and 2.

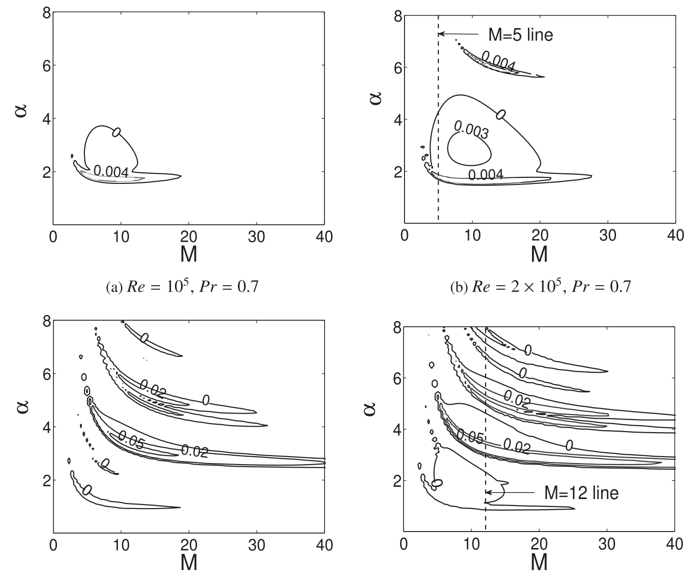

(a) $Re = 10^5$, $Pr = 0.7$ (b) $Re = 2 \times 10^5$, $Pr = 0.7$ (c) $Re = 10^5$, $Pr = 0.2$ (d) $Re = 2 \times 10^5$, $Pr = 0.2$

Fig. 7. Stability diagrams in the $M - \alpha$ plane show that as the Prandtl number is reduced, the growth rates, range of instability in Mach number as well as the number of instability loops increase for all the Reynolds number cases considered.

($\alpha_i < 0$) is bypassed from above. This is identified as branching pattern **C** in Federov and Tumin (2011).

When the modes revert back as shown in Fig. 5(b), they exchange their characteristics. We notice that the peaks in the eigenfunctions appear near the top and bottom wall for the modes 1 and 2 respectively, which is opposite to that observed originally in Fig. 4(a) and (b) before synchronization. This is in contrast to the high Prandtl number case ($= 0.5$), where modes 1 and 2 retain their characteristics past the synchronization point in the cross-over branching.

4.3. Effect of Pr on the branching pattern

For a fixed Mach number and Reynolds number, there exists a distinct Prandtl number that distinguishes the region where modes 1 and 2 cross one another or revert back with increasing wavenumber. This is illustrated in Fig. 6, which plots the threshold Prandtl number as a function of Mach number, at Reynolds numbers of 10^5 and 10^6. When the Prandtl number is higher than the threshold, "cross-over" branching pattern is observed corresponding to the synchronization between the first two acoustic modes. The "revert back" branching pattern is noticed for *Pr* values lower than the threshold. The threshold Prandtl number is found to decrease for higher Reynolds number at high Mach numbers.

As noted earlier, "cross-over" branching between the first two acoustic modes is associated with unstable mode 2 disturbances. On the other hand, mode 1 is destabilized when the acoustic modes undergo a "revert-back" branching. Thus, the threshold Prandtl number for a given Mach and Reynolds number also distinguishes the parameter values where mode 1 or mode 2 will be the dominant instability. Identification of modes causing instability is discussed in detail in the next section.

5. Stability diagrams in the $M - \alpha$ plane

Fig. 7 presents the stability diagram in the Mach number versus wavenumber plane for two-dimensional disturbances at various Reynolds numbers and Prandtl numbers. It shows the growth rate contours of the least stable mode for a range of Mach numbers and wavenumbers. The regions within the loops are unstable with positive growth rates and the region outside is stable. For the two Reynolds numbers considered, it can be observed that as the Prandtl number decreases for a given *Re*, the regions of instability as well as the magnitude of the growth rates increase. For instance, at $Re = 10^5$, as Prandtl number reduces from 0.7 (Fig. 7(a)) to 0.2 (Fig. 7(c)) there are additional loops of instability with higher growth rates. The maximum growth rate increases from 0.004 to 0.05 with the decrease in the Prandtl number value. Hence, for a fixed Reynolds number, the effect of reducing the Prandtl number is destabilizing.

For determining the effect of Reynolds number at a fixed Prandtl number, Fig. 7(a) and (b) are compared. When the Reynolds number increases from 10^5 to 2×10^5 at $Pr = 0.7$, it can be noticed that the size of the instability loops increase, and additional loops of instability are seen at this comparatively high value of Prandtl number. Similar effects are also observed at 0.2 (compare Fig. 7(c) and (d)). Malik et al. (2008) present comparable results for $Pr = 0.72$, at the same Reynolds numbers (10^5 and 2×10^5).

5.1. Identification of the modes causing instability

A high Reynolds number and low Prandtl number lead to large regions of instability in the $M - \alpha$ plane. In order to identify the acoustic modes associated with the various instability loops, we study the case of $Re = 2 \times 10^5$ and $Pr = 0.2$ (Fig. 7(d)). Several instability loops are observed in the Mach number range of 5–40. For Mach numbers beyond 40, the number of instability loops decrease. The only exception is the second loop with maximum growth rate around 0.02 well into the high Mach number range. This is of particular interest because the low value of Prandtl number considered here is expected to occur at low pressure and high temperature conditions, which are encountered during re-entry flight at high Mach number and high altitude.

The variation of growth rate of the least stable mode ($\mathrm{Im}(\omega_{ld})$) with wave number for a fixed Mach number of 12 is plotted in Fig. 8. The values of Reynolds number and Prandtl number match those in Fig. 7(d), and the data is extracted along the dashed line shown in the figure. The highest growth rate is found at a wavenumber of 3.25, corresponding to the second loop in Fig. 7(d). This is caused by acoustic mode 1, with growth rate of around 0.058. The instability peaks due to mode 2 appear at two wavenumbers, namely, 0.96 (lowest loop in Fig. 7(d)) and 5 (third instability loop in Fig. 7(d)). Acoustic modes 3, 4 and 5 also ap-

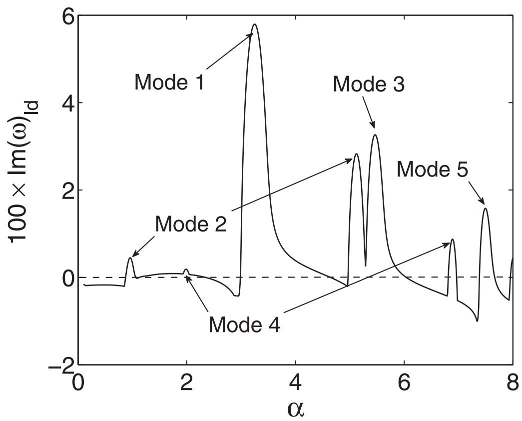

Fig. 8. The dominant unstable acoustic modes at various wave numbers for a Couette flow at $M = 12$, $Pr = 0.2$, and $Re = 2 \times 10^5$ are identified. The instability peaks correspond to synchronizations between acoustic modes.

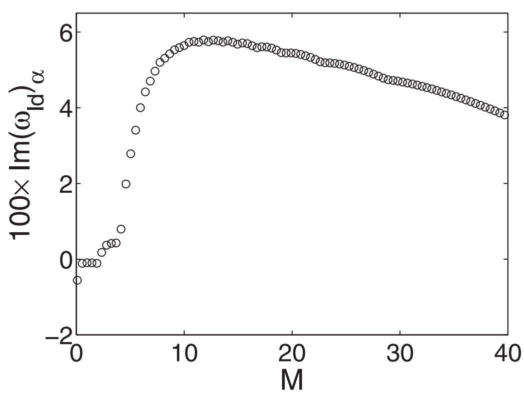

Fig. 9. Maximum growth rate over a range of wavenumbers $(0-8)$ is plotted as a function of M at $Re = 2 \times 10^5$ and $Pr = 0.2$. Mode 1 is the most dominant unstable mode for Mach numbers exceeding 5.

pear as dominant instabilities as discrete peaks around $\alpha = 5.47$, $\alpha = 1.99$ and 6.89, and $\alpha = 7.52$ respectively.

We note that the instability peaks listed above correspond to mode-synchronizations between various acoustic modes. For example, the high growth rate at $\alpha = 3.25$ is due to the synchronization of modes 1 and 2, which is akin to the case presented in Fig. 5. Similarly, the growth rate peak observed around $\alpha = 5$ is due to the synchronization between the second and the fourth acoustic modes.

Fig. 9 presents the variation of maximum growth rate over a range (0–8) of wave numbers for a $Re = 2 \times 10^5$, $\beta = 0$ and $Pr = 0.2$ Couette flow. Mode 1 is the most dominant instability for most of the range of Mach numbers (≥ 5). This is due to the revert back branching on synchronization of modes 1 and 2 (refer Section 4.2). Mode 2 is the most unstable mode in the low Mach number range ($M < 5$) and comes from the bottom instability loop of Fig. 7(d). On the other hand, at high Prandtl numbers, for example at $Pr = 0.72$, mode 2 dominates over the entire range of Mach number $(0.1 - 40)$. In this case, the synchronization between the first two acoustic modes makes mode 2 more unstable, due to the cross-over branching explained in Section 4.1. Malik et al. (2008) also report similar findings for a uniform viscosity and conductivity Couette flow at $Pr = 0.72$.

6. Stability diagrams in the $Re - \alpha$ plane

Fig. 10 presents the stability diagram in the Reynolds number versus wavenumber plane for two Mach numbers 5 and 10, with

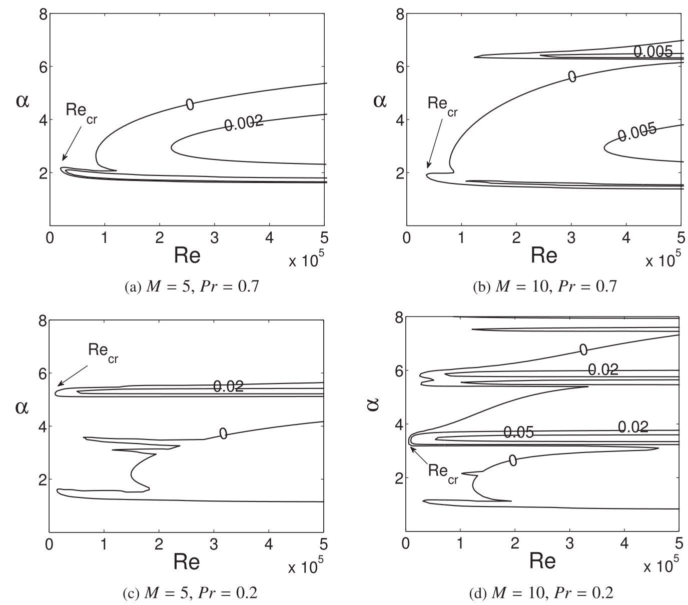

(a) $M = 5$, $Pr = 0.7$
(b) $M = 10$, $Pr = 0.7$
(c) $M = 5$, $Pr = 0.2$
(d) $M = 10$, $Pr = 0.2$

Fig. 10. Stability diagrams in the $Re - \alpha$ plane plotted for two different Mach numbers show that, as Pr is reduced critical Reynolds number also decreases.

Table 1
Critical Reynolds number and corresponding wave number for a uniform viscosity and conductivity plane Couette flow at varying Prandtl numbers and for two Mach numbers.

	M = 5		M = 10	
Pr	Re_{cr}	α_{cr}	Re_{cr}	α_{cr}
0.7	19036	2.16	35680	1.90
0.5	15136	1.98	30042	1.66
0.2	10442	5.22	5232	3.34

different values of Prandtl numbers. For a given Mach number, as Prandtl number is lowered, more instability loops appear in addition to the bottom loop. Also the peak growth rate increases with the reduction in the Prandtl number value. This is more prominent when we compare different Pr cases at $M = 10$. For example, as the Prandtl number is decreased from 0.7 to 0.2, the peak growth rate increases from 0.005 to 0.05. When the two Mach number (5 and 10) cases are compared for a fixed Prandtl number, it can be seen that the peak growth rate increases with increase in Mach number.

The critical Reynolds numbers (Re_{cr}) along with the critical wave numbers (α_{cr}) are listed in Table 1. It can be noted that, for both $M = 5$ and $M = 10$, critical Reynolds number decreases monotonically as the Prandtl number is reduced. However, the variation of critical Reynolds number is not monotonic with Mach number. This is also observed in Malik et al. (2008) for a Couette flow with both uniform as well as non-uniform shear. For Prandtl numbers of 0.7 and 0.5, the critical Reynolds number increases as Mach number is increased. However, when Pr reaches a value of 0.2, the critical Reynolds number attains a lower value for $M = 10$ compared to $M = 5$. Therefore Mach number has a dual role of stabilizing and destabilizing the flow, depending on the Prandtl number.

7. Effect of heating/cooling the lower wall

The destabilizing effect of wall cooling has been reported earlier; see the works of Lees (1947); Mack (1984) and Mack (1993). In this section, we examine the effect of variation in Prandtl number at different wall cooling/heating conditions. For this, we choose

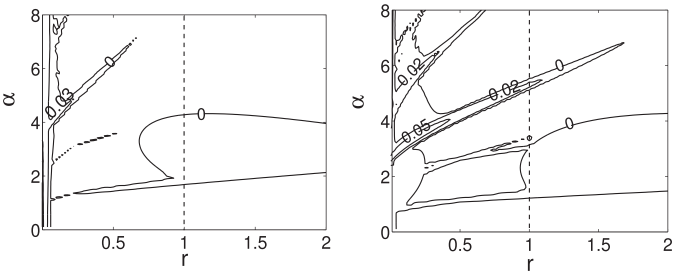

(a) $Pr = 0.7$ (b) $Pr = 0.2$

Fig. 11. Growth rate contours plotted as a function of wall cooling parameter ($= r$) and disturbance wavenumber at $M = 5$, $\beta = 0$ and $Re = 2 \times 10^5$. Data shows that wall cooling increases the regions of instability with higher growth rates, and reducing the Prandtl number increases the maximum growth rate in each loop.

a parameter which is the ratio ($= r$) of bottom wall temperature (T_w) to the recovery temperature (T_r). The recovery temperature is a function of Mach number and Prandtl number and is defined as, $T_r = 1 + \frac{(\gamma-1)}{2} Pr M^2$. The lower wall is defined as cold or hot, if the wall temperature is less than or greater than T_r respectively. If the value of bottom wall temperature is equal to the recovery temperature ($r = 1$), then it is the case of an adiabatic wall.

Fig. 11 shows the variation of the maximum growth rate in the $r - \alpha$ plane for $M = 5$ and $Re = 2 \times 10^5$ case, at different Prandtl numbers. We notice that lowering the bottom wall temperature leads to higher growth rates for both the Prandtl numbers, while heating has a mild stabilizing effect. It can be observed that when cooling increases (r decreases), additional instability loops appear, and the maximum growth rate also increases. Also, the location of the peaks shift to a lower wave number, as cooling is increased.

The loops and spikes in Fig. 11 conform to different instability loops in the corresponding $M - \alpha$ diagram. For instance, the growth rates observed along $r = 1$ line in Fig. 11(a) and (b) correspond to the growth rates along a line at $M = 5$ in Fig. 7(b) and (d) respectively. The values of wavenumber ranging from $1 - 4$ at $r = 1$ in Fig. 11(b) corresponds to the lower instability loop in Fig. 7(d). Also, the spike that appears around $\alpha = 5$ and $r = 1$ in Fig. 11(b) corresponds to the second instability loop of Fig. 7(d) with growth rate around 0.02.

8. Conclusion

We have investigated the effect of Prandtl number on the stability of a uniform viscosity and conductivity Couette flow at high Mach numbers. Prandtl number values are systematically varied from $0.2 - 0.9$ by changing the relative magnitudes of viscosity and conductivity, and a temporal linear stability analysis is performed. We find that decreasing the Prandtl number has a destabilizing effect on the flow at all Mach and Reynolds numbers. The critical Reynolds number is significantly reduced, by up to an order of magnitude, especially at high Mach numbers. The flow is more unstable at lower Prandtl numbers irrespective of the wall boundary conditions (cold/hot/adiabatic). High growth rates with additional instability loops are observed in the stability diagrams as the Prandtl number is decreased.

It is found that the local peaks in the growth rates are due to the synchronization between the acoustic modes. Two types of branching patterns are seen at mode-synchronization, namely, cross-over and revert-back. Cross-over branching between the first two acoustic modes occurs at relatively high Prandtl numbers. It is found to destabilize mode 2 acoustic instabilities, and the mode shapes are retained through the synchronization process. By comparison, revert-back synchronization is usually noticed at relatively low Prandtl numbers. It results in high mode 1 growth rates, and the even and odd acoustic mode shapes are exchanged past the synchronization point. We compute the threshold Prandtl number that distinguishes the two branching patterns and thus determines the dominant instability mode in compressible Couette flow. In summary, we find that the Prandtl number can play a crucial role in the stability of high Mach number wall-bounded flows. We hope that this paper will motivate studies on the effect on Prandtl number in more complex flows relevant for high-speed applications.

Appendix

The linear stability equations for the perturbations can be expressed as a generalized eigenvalue problem, given by,

$$\begin{bmatrix} B_{11} & B_{12} & B_{13} & B_{14} & B_{15} \\ B_{21} & B_{22} & B_{23} & B_{24} & B_{25} \\ B_{31} & B_{32} & B_{33} & B_{34} & B_{35} \\ B_{41} & B_{42} & B_{43} & B_{44} & B_{45} \\ B_{51} & B_{52} & B_{53} & B_{54} & B_{55} \end{bmatrix} \begin{Bmatrix} \hat{u} \\ \hat{v} \\ \hat{w} \\ \hat{\rho} \\ \hat{T} \end{Bmatrix} = \omega \begin{bmatrix} 1 & 0 & 0 & 0 & 0 \\ 0 & 1 & 0 & 0 & 0 \\ 0 & 0 & 1 & 0 & 0 \\ 0 & 0 & 0 & 1 & 0 \\ 0 & 0 & 0 & 0 & 1 \end{bmatrix} \begin{Bmatrix} \hat{u} \\ \hat{v} \\ \hat{w} \\ \hat{\rho} \\ \hat{T} \end{Bmatrix} \tag{12}$$

The rows in the above system correspond to the three momentum, continuity and energy equations respectively. The elements of the matrix B are:

$$B_{11} = \alpha\bar{u} - i\frac{\left[\bar{\mu}\left(\alpha^2 + \beta^2\right) + \alpha^2\left(\bar{\mu} + \bar{\lambda}\right) - \bar{\mu}_y D - \bar{\mu} D^2\right]}{\bar{\rho} Re},$$

$$B_{12} = -i\bar{u}_y - \alpha\frac{\left[\bar{\mu}_y + \left(\bar{\lambda} + \bar{\mu}\right) D\right]}{\bar{\rho} Re},$$

$$B_{13} = -i\alpha\beta\frac{\left(\bar{\lambda} + \bar{\mu}\right)}{\bar{\rho} Re},$$

$$B_{14} = \frac{\alpha\bar{T}^2}{\gamma M^2},$$

$$B_{15} = \frac{\alpha}{\gamma M^2} + i\frac{\left[\bar{u}_{yy}\bar{\mu}_T + \bar{u}_y\bar{T}_y\bar{\mu}_{TT} + \bar{u}_y\bar{\mu}_T D\right]}{\bar{\rho} Re},$$

$$B_{21} = -\alpha\frac{\left[\bar{\lambda}_y + \left(\bar{\lambda} + \bar{\mu}\right) D\right]}{\bar{\rho} Re},$$

$$B_{22} = \alpha\bar{u} + i\frac{\left[\left(\bar{\mu}_y + \bar{\lambda}_y\right) D - \bar{\mu}\left(\alpha^2 + \beta^2\right) + \left(\bar{\mu} + \bar{\lambda}\right) D^2 + \bar{\mu}_y D + \bar{\mu} D^2\right]}{\bar{\rho} Re},$$

$$B_{23} = -\beta\frac{\left[\bar{\mu}_y + \left(\bar{\lambda} + \bar{\mu}\right) D\right]}{\bar{\rho} Re},$$

$$B_{24} = -i\frac{\left(\bar{T}_y + \bar{T} D\right)}{\bar{\rho}\gamma M^2},$$

$$B_{25} = -i\frac{\left(\bar{\rho}_y + \bar{\rho} D\right)}{\bar{\rho}\gamma M^2} - \frac{\alpha\bar{u}_y\bar{\mu}_T}{\bar{\rho} Re},$$

$$B_{31} = -i\alpha\beta\frac{\left(\bar{\lambda} + \bar{\mu}\right)}{\bar{\rho} Re},$$

$$B_{32} = -\beta\frac{\left[\bar{\mu}_y + \left(\bar{\lambda} + \bar{\mu}\right) D\right]}{\bar{\rho} Re},$$

$$B_{33} = \alpha\bar{u} - i\frac{\left[\bar{\mu}\left(\alpha^2 + \beta^2\right) + \beta^2\left(\bar{\mu} + \bar{\lambda}\right) - \bar{\mu}_y D - \bar{\mu} D^2\right]}{\bar{\rho} Re},$$

$$B_{34} = \frac{\beta\bar{T}^2}{\gamma M^2},$$

$$B_{35} = \frac{\beta}{\gamma M^2},$$

$$B_{41} = \alpha\bar{\rho},$$
$$B_{42} = -i(\bar{\rho}_y + \bar{\rho}D),$$
$$B_{43} = \beta\bar{\rho},$$
$$B_{44} = \alpha\bar{u},$$
$$B_{45} = 0,$$
$$B_{51} = \alpha(\gamma-1)\bar{T} + i\frac{2(\gamma-1)M^2\bar{\mu}\bar{u}_y D}{\bar{\rho}Re},$$
$$B_{52} = -i\bar{T}_y - i(\gamma-1)\bar{T}D - \frac{2\alpha(\gamma-1)M^2\bar{\mu}\bar{u}_y}{\bar{\rho}Re},$$
$$B_{53} = \beta(\gamma-1)\bar{T},$$
$$B_{54} = 0,$$
$$B_{55} = \alpha\bar{u} + i\frac{\left[\bar{T}_{yy}\bar{k}_T + \bar{T}_y^2\bar{k}_{TT} + 2\bar{T}_y\bar{k}_T D - \left(\alpha^2+\beta^2\right)\bar{k} + \bar{k}D^2 + (\gamma-1)M^2\,Pr\,\bar{u}_y^2\bar{\mu}_T\right]}{\bar{\rho}\,Re\,Pr}.$$

Here, D is the differential operator; subscripts y and T denote the derivatives with respect to y and $\bar{T}$ respectively.

References

Capitelli, M., Colonna, G., Gorse, C., D'Angola, A., 2000. Transport properties of high temperature air in local thermodynamic equilibrium. Eur. Phys. J. D-Atomic, Mol. Optical Plasma Phys. 11, 279–289.

Duck, P.W., Erlebacher, G., Hussaini, M.Y., 1994. On the linear stability of compressible plane Couette flow. J. Fluid Mech. 258, 131–165.

Federov, A.V., Tumin, A., 2011. High-speed boundary-layer instability: Old terminology and a new framework. AIAA J. 49, 1647–1657.

Franko, K.J., MacCormack, R.W., Lele, S.K., 2010. Effects of chemistry modeling on hypersonic boundary layer linear stability prediction. AIAA Paper No. 2010–4601.

Hu, S., Zhong, X., 1998. Linear stability of viscous supersonic plane Couette flow. Phys. Fluids 10, 709.

Hudson, M.L., Chokani, N., Candler, G.V., 1997. Linear stability of hypersonic flow in thermochemical nonequilibrium. AIAA J. 35, 958–964.

Johnson, H.B., Seipp, T.G., Candler, G.V., 1998. Numerical study of hypersonic reacting boundary layer transition on cones. Phys. Fluids 10, 2676.

Lees, L., 1947. The stability of the laminar boundary layer in a compressible fluid. Report No. 876, NACA,Washington.

Lyttle, I.J., Reed, H.L., 2005. Sensitivity of second-mode linear stability to constitutive models within hypersonic flow. AIAA Paper No. 2005-889.

Mack, L.M., 1984. Boundary-layer linear stability theory. Special Course on Stability and Transition of Laminar Flow. Pp. 3/181. AGARD Rep. No. 709.

Mack, L.M., 1987. Review of linear compressible stability theory. In: Stability of time dependent and spatially varying flows, New York, pp. 164–187.

Mack, L.M., 1993. Effect of cooling on boundary-layer stability at Mach number 3. In: Ashpis, D., Gatski, T., Hirsh, R. (Eds.), Instabilities and Turbulence in Engineering Flows. Boston: Kluwer Academic Publishers, pp. 175–188.

Malik, M., Dey, J., Alam, M., 2008. Linear stability, transient energy growth, and the role of viscosity stratification in compressible plane Couette flow. Phys. Rev. E 77, 036322.

Malik, M.R., 1990. Numerical methods for hypersonic boundary layer stability. J. Comput. Phys. 86, 376–413.

Malik, M.R., Anderson, E.C., 1991. Real gas effects on hypersonic boundary layer stability. Phys. Fluids 3, 803.

Ramachandran, A., Saikia, B., Sinha, K., Govindarajan, R., 2015. Linear stability of high-speed boundary layer flows at varying Prandtl numbers. In: 45th AIAA Thermophysics Conference. AIAA Paper No. 2015–2320.

Reshotko, E., 1960. Stability of the compressible laminar boundary layer. California Institute of Technology. Phd thesis.

Saikia, B., Ramachandran, A., Sinha, K., Govindarajan, R., 2016. Effects of viscosity and conductivity stratification on the linear stability and transient growth of compressible Couette Flow. Physics of Fluids (under review).

Sameen, A., Govindarajan, R., 2007. The effect of wall heating on instability of channel flow. J. Fluid Mech. 577, 417–442.

Trefethen, L.N., 2000. Spectral methods in MATLAB, vol.10. Siam, Philadelphia, pp. 51–55.

Wall, D.P., Wilson, S.K., 1997. The linear stability of flat-plate boundary-layer flow of fluid with temperature-dependent viscosity. Phys. Fluids 9, 2885.

Xie, Z., Girimaji, S.S., 2014. Instability of Poiseuille flow at extreme Mach numbers: Linear analysis and simulations. Phys. Rev. E 89, 043001.